Maxwell and non-Maxwell behavior of electron energy distribution function under expanding plasma jet conditions: The role of electron-electron, electron-ion, and superelastic electronic collisions under stationary and time-dependent conditions

M. Capitelli,[1] G. Colonna,[1] A. Gicquel,[2] C. Gorse,[1] K. Hassouni,[2] and S. Longo[1]

[1]*Centro di Studio per la Chimica dei Plasmi del CNR and Dipartimento di Chimica dell'Università di Bari, 70126 Bari, Italy*

[2]*Laboratoire des Interactions Moléculaires et des Hautes Pressions, Université de Paris–Nord, CNRS, 93430 Villetaneuse, France*

(Received 18 October 1995; revised manuscript received 4 March 1996)

A stationary and a time-dependent Boltzmann equation including elastic, inelastic, and superelastic terms has been solved for conditions typically met in expanding the Ar-H_2 plasma jet, i.e., for large ionization degrees and large concentrations of electronically excited states. The results show that the stationary electron-energy distribution functions (EEDFs) in the presence of electron-electron and electron-ion (e-i) Coulomb collisions evolve to the bi-Maxwellian distribution function in which the lower temperature is determined by e-i collisions, and the higher one by superelastic electronic collisions. On the other hand, the time-dependent EEDF clearly shows long plateaus generated by superelastic electronic collisions for times comparable to the expansion ones. [S1063-651X(96)08108-1]

PACS number(s): 52.20.−j, 52.30.−q

I. INTRODUCTION

The role of electron-electron collisions in giving Maxwellian characteristics to the electron-energy distribution function (EEDF) under discharge conditions has been studied by different authors [1–4]. It is commonly believed that ionization degrees (n_e/N, with n_e electron density and N total neutral density) of the order of 10^{-4}–10^{-3} can be sufficient to give the Maxwellian characteristics of the EEDF for different gases and different plasma conditions.

In a recent work by Colonna *et al.* [5] it was shown that an ionization degree of the order of 10^{-3} is still unable to completely give Maxwellian characteristics to the EEDF in N_2 excited post discharges. This behavior has been attributed to the presence of electronically and vibrationally excited states. Such states distort the EEDF from a Maxwellian, thus reducing the effectiveness of e-e collisions to thermalize the distribution. This effect is more important for higher concentrations of electronically excited states.

A natural question arises about the experimental conditions necessary to achieve very high concentrations of excited states. Recently, Otorbaev *et al.* [6] showed that such a possibility exists for expanding plasma jet conditions. These authors were able to measure excited-state concentrations, electron and ion densities, electron and gas temperatures, and dissociation degrees at different positions of expanding arc. Part of these data, which represent the input of our calculations, has been reproduced in Table I.

In the experiment of Ref. [6] a relatively high electron density, Ar* metastable concentration, and a very low electron temperature were observed. The large concentration of Ar* metastable states together with the low T_e values is the ideal regime for the action of superelastic electronic collision:

$$e + \mathrm{Ar}^* \rightarrow e + \mathrm{Ar}, \tag{1}$$

while electron-electron and electron-ion collisions should ensure the Maxwellian characteristics of EEDFs as implicitly assumed in Ref. [6].

Superelastic electronic collisions should move low-energy electrons to higher energies: in particular, one should have production of electrons at 11.55 and 23.10 eV and so on as a result of process (1) (11.55 eV is the energy of the Ar* metastable state with respect to the ground state). These electrons are then redistributed by elastic (including electron-ion), inelastic, and electron-electron collisions, the last trying to give the Maxwellian characteristics to the resulting EEDFs.

The aim of this work is to show that, in an expanding arc, the EEDF keeps the memory of process (1) despite the large ionization degrees characterizing the whole flow field. It is also to investigate the effect of this process on the rate constants of the main chemical reactions and on the energy-transfer mechanism in the arc jet. Unlike our previous works, this investigation deals with an expanded arc jet characterized by a high ionization degree. Furthermore, this system has been extensively investigated from the experimental point of view. This enables us to study the dynamics of electron-electron and superelastic collisions with input parameters determined experimentally. Therefore, the present study, even though still parametric, can be considered more realistic compared to our previous works. Moreover, the arc expanding conditions describe situations that are of interest in hypersonic flows.

The outline of the paper is as follows. In Sec. II we illustrate the method of calculation based on the solution of an appropriate Boltzmann equation either for stationary or for nonstationary conditions (time dependent) including the elementary processes reported above. The results obtained by solving this equation for the experimental conditions of Ref. [6] are discussed in Sec. III. Finally, the main conclusions obtained from the analysis of the theoretical results and from the comparison between these results and the experimental ones are reported in Sec. IV.

TABLE I. Typical plasma parameters on the axis of the expanding cascaded arc for differential axial positions (Ar-H_2 mixture 98.6:1.4).

Distance (cm)	2	4	7
Electron density (cm^{-3})	2.9×10^{13}	2.2×10^{13}	3.0×10^{13}
Argon-ion density (cm^{-3})	2.8×10^{13}	2.2×10^{13}	2.9×10^{13}
Proton density (cm^{-3})	0.8×10^{12}	0.6×10^{12}	0.8×10^{12}
Electron temperature (K)	1 500	2 400	2 500
Neutral-particle density (cm^{-3})	10^{15}	0.7×10^{15}	10^{15}
Heavy-particle temperature (K)	3 000	3 000	3 000
Ar* concentration (cm^{-3})	2.7×10^{12}	4.1×10^{11}	2.4×10^{11}
H($n=2$) concentration (cm^{-3})	4.9×10^{7}	1.5×10^{9}	2.4×10^{9}
H($n=3$) concentration (cm^{-3})	2.9×10^{7}	2.1×10^{7}	2.2×10^{7}
H_2 dissociation degree (%)		22	10
T_{e1} (K)	2 650	2 200	2 060
T_{e2} (K)	14 500	11 300	5 600
T_{e3} ($=\frac{2}{3}\langle\epsilon\rangle$, K)	15 100	11 900	6 050
$P_{\rm rec}(T_{e1})$ (eV cm^{-3} s^{-1})	7.5×10^{16}	7.5×10^{16}	2.6×10^{17}
$P_{\rm rec}(T_{e2})$ (eV cm^{-3} s^{-1})	3.6×10^{13}	4.8×10^{13}	2.9×10^{15}
$P_{\rm rec}(T_{e3})$ (eV cm^{-3} s^{-1})	3.0×10^{13}	3.8×10^{13}	2.0×10^{15}
$P_{\rm sup}$ (eV cm^{-3} s^{-1})	6.5×10^{17}	6.4×10^{16}	3.2×10^{16}

II. METHOD OF CALCULATION

The method of calculation has been widely discussed in previous works [1,4,5]. It consists in solving an appropriate Boltzmann equation, which can be written in an implicit form as

$$\frac{\partial n(\varepsilon,t)}{\partial t}=\frac{\partial J_f}{\partial \varepsilon}+\frac{\partial J_{el}}{\partial \varepsilon}+\frac{\partial J_{e-e}}{\partial \varepsilon}+\frac{\partial J_{e-i}}{\partial \varepsilon}+\left(\frac{\partial n}{\partial \varepsilon}\right)_{\rm in}+\left(\frac{\partial n}{\partial \varepsilon}\right)_{\rm sup}, \tag{2}$$

where $n(\varepsilon,t)d\varepsilon$ is the electron density with energy between ε and $\varepsilon+d\varepsilon$ at time t. The first term on the right-hand side of Eq. (1) represents the flux of electrons in the energy space due to the electric field. The other terms denote the fluxes due, respectively, to elastic (electron-neutral), electron-electron, electron-ion, inelastic, and superelastic collisions. The expressions of the different terms appearing in Eq. (2) may be found in Refs. [1,4,5]. Note that the electron-ion term has been treated as the electron-neutral elastic collision with a Coulomb cross section, i.e.,

$$\sigma_{e-i}(\varepsilon)=\frac{9\pi^{3/2}e^4\ln\Lambda}{8\varepsilon^2}, \tag{3}$$

where e is the electron charge and Λ is the ratio between the Debye length and the averaged closest impact parameter.

The EEDF was investigated in the energy range 0 eV$<\varepsilon<$25 eV. The Boltzmann equation was written in a discrete form using a central difference operator on a 250-mesh grid. This leads to a set of 250 nonlinear ordinary differential equations, which could be written in matrix form as follows:

$$f(d\mathbf{n}/dt)=\underline{C}\mathbf{n}, \tag{4}$$

where $\mathbf{n}$ is a vector, the components of which are the EEDF values at the different energy grid points $\{\mathbf{n}=[n(\varepsilon_1),n(\varepsilon_i),\ldots,n(\varepsilon_1)]\}$. $C=(c_{ij})$ is the nonlinear collision matrix, which takes into account the elastic, inelastic, superelastic, and electron-electron (e-e) collisions [1]. This system of equations was solved using a time-implicit predictor-corrector method that is, in principle, unconditionally stable. It allows the use of large time step and insures a reasonable computation time. However, this method does not give an accurate description of the EEDF time evolution, and only the steady-state solution is accurately calculated.

The time-dependent solution of the Boltzmann equation was, on the contrary, obtained by using the Rockwood algorithm [1]. A very short time step ($t=5\times10^{-11}$ s) was used to avoid numerical instabilities due to e-e collisions.

Elastic, inelastic, and superelastic collisions involving H_2 and H systems are the same as discussed in Ref. [7]. The relevant elastic and inelastic cross sections have been taken from the compilation of Buckmann and Phelps [8] for H_2 and from Ref. [9] for H, while the cross sections for superelastic collisions have been derived from a detailed balance principle.

In addition to process (1), we have considered superelastic electronic collisions coming only from excited atomic hydrogen ($n=2$, $n=3$) and vibrationally excited molecules i.e., the processes

$$e+\mathrm{H}(n=2;n=3)\rightarrow e+\mathrm{H}(n=1), \tag{5}$$

$$e+\mathrm{H}_2(v=1,2,3)\rightarrow e+\mathrm{H}_2(v=0), \tag{6}$$

where n and v are, respectively, the principal quantum number of excited atoms and the vibrational quantum number of molecules.

For Ar we include, besides the elastic, superelastic [process (1)] and the ionization terms, two electronic inelastic terms, one leading to the metastable state, i.e., the reverse of

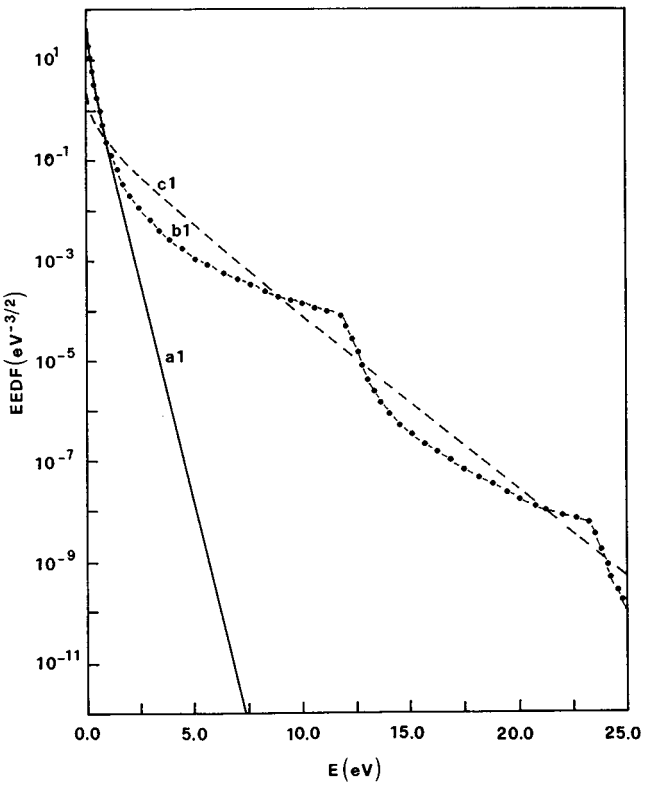

FIG. 1. EEDF calculated by solving the Boltzmann equation (2) with $\partial n/\partial t=0$ for $x=20$ mm. The three curves ($a1$), ($b1$), and ($c1$) refer, respectively, to hypotheses $a-c$ in the text for the first position (a: elastic and inelastic processes; b:a plus superelastic collisions; c:b plus e-e collisions).

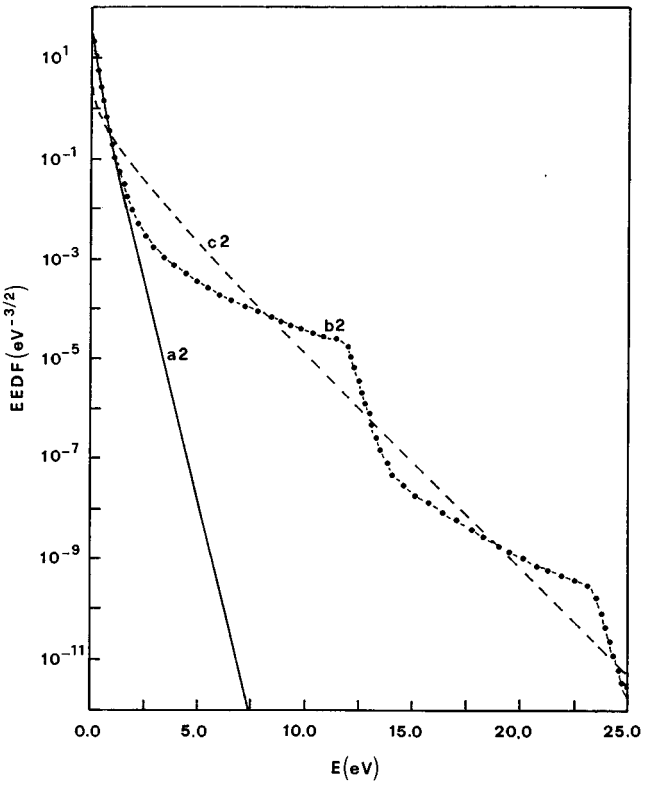

FIG. 2. EEDF calculated by solving the Boltzmann equation (2) with $\partial n/\partial t=0$ for $x=40$ mm. The three curves ($a2$), ($b2$), and ($c2$) refer, respectively, to hypotheses $a-c$ in the text for the second position (a: elastic and inelastic processes; b:a plus superelastic collisions; c:b plus e-e collisions).

process (1), the other to the excitation over all the remaining excited states of Ar. The relevant cross sections are those included in the ELENDIF program of Morgan and Penetrante [10].

The concentrations of Ar and H excited species are the experimental ones reported in Table I, while Boltzmann distributions at $T=T_v=3000$ K have been considered for H_2. It should be noted that these concentrations, as well as those of electrons and ions, remain fixed during the solution of the Boltzmann equation, for either stationary or time-dependent conditions. This is indeed an approximation and a full modeling of the arc jet should include the coupling of the species kinetic equations, the electron Boltzmann equation, and the fluid dynamic equations in the whole plasma flow field. Such considerations are outside the scope of this work, the main objective of which is to investigate the effects of the respective weights of the different collision processes on EEDF, the reaction-rate coefficients and the energy-transfer mechanisms.

III. RESULTS

Stationary EEDF's for the three positions of Table I have been reported in Figs. 1–3. Each of these figures includes the EEDF calculated by considering the following processes in the Boltzmann equation.

(a) Only inelastic and electron–heavy particle elastic processes (including electron-ion) as well as superelastic vibrational collisions.

(b) As in (a) plus superelastic electronic collisions.

(c) As in (b) plus electron-electron collisions.

By comparing (a) and (b) for the three positions, we can see a strong change of the EEDF when taking into account the superelastic electronic collisions that generate a high electron population for energy values greater than 2.5 eV. Indeed, the EEDF of case (b) presents large plateaus. The electron populations corresponding to these plateaus decrease when going downstream from the arc jet (from position 1 to position 3) as a result of the corresponding decrease in the concentration of excited states. It should be noted that these plateaus are essentially due to Ar* metastable states. Collisions coming from hydrogen-excited states contribute only to a minor extent (approximately in the same energy range) due to their small concentrations as compared with Ar* (see Table I).

The insertion of electron-electron collision terms in the Boltzmann equation completely destroys the long plateaus generated by superelastic electronic collisions for the first two positions [see Figs. 1(c) and 2(c)]. Similar considerations apply for EEDF's relative to the third position. In this case, the action of electron-electron collisions is not important enough to completely remove the plateaus, which still persist in the energy range 10–12.5 eV.

In general, the effect of e-e collisions is to spread out the electrons belonging to the plateau in a much more regular way. As a final result, we can note for the first two positions a bi-Maxwellian behavior of EEDF. The first Maxwellian part of the EEDF, which includes only very low-energy elec-

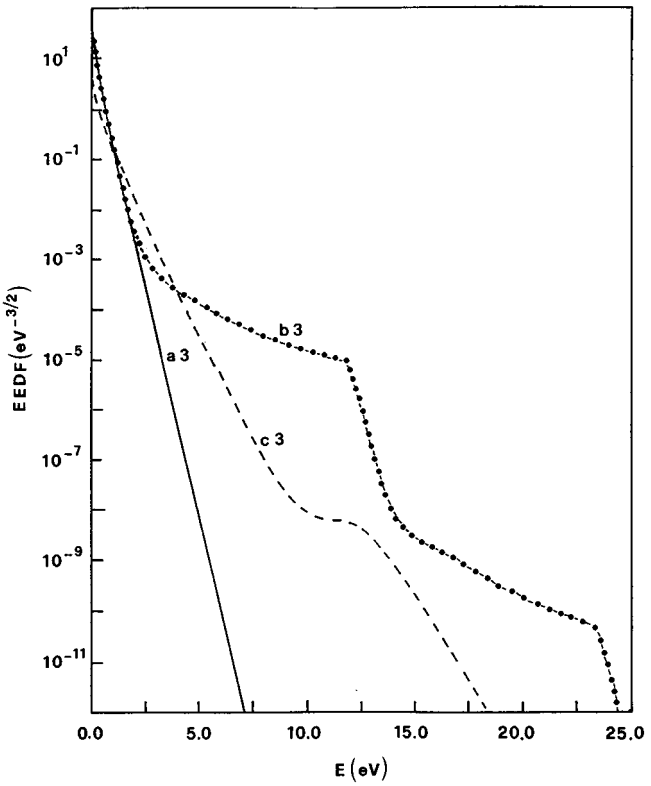

FIG. 3. EEDF calculated by solving the Boltzmann equation (2) with $\partial n/\partial t=0$ for $x=70$ mm. The three curves ($a3$), ($b3$), and ($c3$) refer, respectively, to hypotheses $a-c$ in the text for the third position (a: elastic and inelastic processes; b:a plus superelastic collisions; c:b plus e-e collisions).

trons ($\epsilon \ll 1$ eV) is characterized by a very small electron temperature T_{e1}, while the second part extends from 1 to 25 eV, being characterized by a moderate electron temperature ($T_{e2}>1$ eV). The first Maxwellian part of the distribution is dominated by the strong electron-ion cross section, which is able to rapidly cool the distribution. The second part of the distribution is dominated by superelastic electronic collisions and by the redistribution of electrons through e-e collisions. Similar considerations apply for the EEDF relative to the third position. However, in this case, only a small difference is obtained between the slopes of the first two Maxwellian parts of the EEDF ($T_{e1}=2060$ K and $T_{e2}=5600$ K) and the plateau due to superelastic collisions is not completely removed.

To better understand the role of the different processes in affecting EEDF's we have reported in Fig. 4 the cross sections for the Ar system. Note that these cross sections in the case of e-i and superelastic processes have been respectively multiplied by the ionization degree and by the molar fraction of excited states (the reported values correspond to the first position).

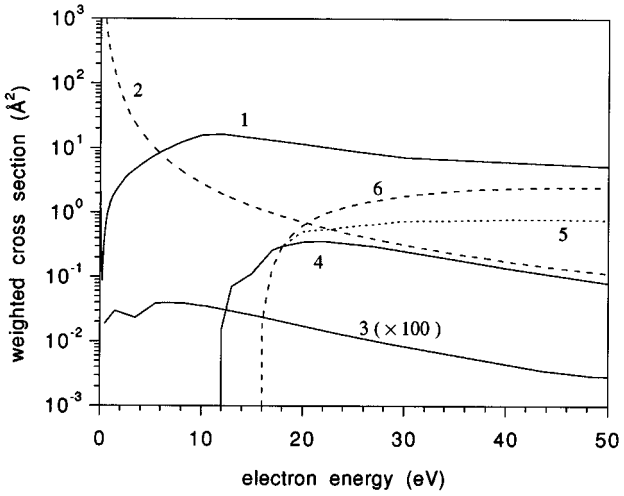

FIG. 4. Elastic, inelastic and superelastic cross sections for the Ar system (the e-i and superelastic cross sections have been respectively multiplied for the molar fraction of A_r^+ and A_r^* relative to the first position); curves: 1 represents electron-Ar momentum transfer; 2 represents electron-ion; 3 represents superelastic; 4 represents metastable excitation; 5 represents lumped level excitation; and 6 represents ionization.

Inspection of Fig. 4 shows that, at very low-energy values, e-i processes dominate the cooling of EEDF's, while above 2 eV the cooling is dominated by an electron-neutral momentum transfer process. In all the investigated cases the superelastic processes (mainly from Ar*) are the only processes that heat the EEDF. It is balanced by elastic (e-i,e-M) processes at low electron energy and by electron-neutral momentum transfer and inelastic collisions at high energy. As a result of the interplay of these processes, we obtain the EEDF reported in Figs. 1–3. Note also that e-e collisions do not change the energy balance of the EEDF; their role is to spread electrons over all distributions.

The bi-Maxwellian character of the EEDF can, therefore, be ascribed to the interplay of e-i, e-e, and superelastic collisions for the very low-energy part of the distribution ($\epsilon \ll 1$ eV) and to the interplay of all processes for the other part of the distribution. Note that even if all the processes are balanced, the fact that ion and metastable populations are out of equilibrium leads to non-Maxwell distribution functions.

TABLE II. Calculated rate coefficients for e-Ar atom processes (cm^3 s^{-1}). Letters a, b, c refer to the hypotheses, as in the text and figures, numbers 1, 2, 3 to the three positions $x=2$, 4, 7 cm respectively. m is the metastable-state excitation, sup is the metastable-state de-excitation (superlastic collision), e is the sum of remaining excitation processes, while i is the ionization. Numbers in brackets represent powers of 10.

	$a1$	$b1$	$c1$	$a2$	$b2$	$c2$	$a3$	$b3$	$c3$
K_m	0.58[−29]	0.31[−12]	0.63[−12]	0.58[−29]	0.49[−13]	0.52[−13]	0.19[−29]	0.18[−13]	0.34[−15]
K_{sup}	0.21 [−9]	0.32 [−9]	0.72 [−9]	0.21 [−9]	0.24 [−9]	0.61 [−9]	0.21 [−9]	0.22 [−9]	0.39 [−9]
K_e	0.10[−28]	0.47[−12]	0.93[−12]	0.10[−28]	0.75[−13]	0.77[−13]	0.33[−29]	0.27[−13]	0.50[−15]
K_1	0.19[−51]	0.38[−13]	0.99[−13]	0.16[−51]	0.23[−14]	0.40[−14]	0.20[−51]	0.38[−15]	0.44[−17]

TABLE III. Calculated rate coefficients for e-H_2 processes ($cm^3\ s^{-1}$). Letters a, b, c refer to the hypotheses as in the text and figures, numbers 1, 2, 3 to the three positions $x=2$, 4, 7 cm, respectively. Symbols indicate the final molecular state, while i is the ionization. Numbers in brackets represent powers of 10.

	$a1$	$b1$	$c1$	$a2$	$b2$	$c2$	$a3$	$b3$	$c3$
$b\ ^3\Sigma$	0.18[−23]	0.12[−10]	0.84[−11]	0.18[−23]	0.30[−11]	0.12[−11]	0.60[−24]	0.12[−11]	0.38[−14]
$b\ ^1\Sigma$	0.20[−27]	0.15[−11]	0.13[−11]	0.20[−27]	0.32[−12]	0.13[−12]	0.63[−28]	0.13[−12]	0.81[−15]
$c\ ^3\Sigma$	0.16[−28]	0.81[−12]	0.11[−11]	0.16[−28]	0.15[−12]	0.10[−12]	0.52[−29]	0.57[−13]	0.73[−15]
$a\ ^3\Sigma$	0.27[−28]	0.36[−12]	0.70[−12]	0.26[−28]	0.55[−13]	0.63[−13]	0.87[−30]	0.19[−13]	0.46[−15]
K_i	0.67[−49]	0.20[−13]	0.61[−13]	0.59[−49]	0.12[−14]	0.27[−14]	0.60[−49]	0.20[−15]	0.40[−17]

In all the reported cases the EEDF keeps the memory of superelastic electronic collisions even though, in the presence of e-e and e-i collisions, the plateaus generated by these collisions have been smoothed towards Maxwell distribution functions. This point can be better understood by inspection of Table II(a–c), where we have reported the rate coefficients corresponding to the excitation and to the ionization of Ar, H_2, and H species for the three cases investigated in Figs. 1–3. These rates were obtained by convolution of EEDF's with the appropriate cross sections.

We can see that inclusion of superelastic electronic collisions increases by numerous orders of magnitude the relevant coefficients as compared with the corresponding results obtained by neglecting these collisions (compare the relevant a and b columns). On the other hand, inclusion of e-e collisions does not appreciably change the rate coefficients; they only smooth the structures created by superelastic electronic collisions without modifying their role in changing the relevant rate coefficients (compare the relevant b and c columns). The small differences between the rates obtained according to b and c hypotheses should be examined in light of the accuracy of the cross sections used. Use of a better set of cross sections for inelastic processes in argon can change the absolute rates of the relevant processes without modifying the qualitative trend reported in Tables II–IV.

It should be interesting now to compare the present electron temperatures with those measured by Otarbaev *et al.* [6]. In Table I we show this comparison. In particular, we compare three different theoretical results with the experimental one. The three theoretical T_e values refer to the first (T_{e1}) and second (T_{e2}) Maxwellian parts of the distribution functions of the relevant figures, while the third value is calculated as $T_{e3}=\frac{2}{3}\langle\epsilon\rangle$, where $\langle\epsilon\rangle$ is the average energy of the full distribution function.

We can see that only T_{e1} values are in acceptable agreement with the experimental values, while T_{e2} and T_{e3} largely exceed them. One possible explanation of this behavior is that the experimental setup samples only the low-energy electrons, those belonging to the first Maxwellian part of the EEDF (T_{e1}). The Thompson-Rayleigh scattering method, used in the experiments, is essentially calibrated to sample the low-energy part of Maxwell distribution functions.

The discrepancy between the theoretical (T_{e3}) and measured electron temperatures may be attributed to other cooling mechanisms, which are not considered in the present Boltzmann analysis and should be taken into account. One possibility would be the insertion of a macroscopic term associated with the thermal conductivity of electrons through strong electron temperature gradients. We have to point out, in connection with this mechanism, that Meulembroeks *et al.* [11] have rationalized their experiments by using a one-dimensional two-gas (electrons and neutral) model. In this model, the electron-energy-source term took into account the electron–heavy-particle elastic collisions and heat conduction flux as cooling processes, while the heating of electrons was only attributed to the three-body recombination

$$e+\mathrm{Ar}^+ + e \rightarrow \mathrm{Ar}^* + e \tag{7}$$

with a rate coefficient k_{rec} given by $k_{\mathrm{rec}}=3.3\times10^{-9}\times T_e^{-9/2}$ ($cm^6\ s^{-1}$ and T_e given in K). These authors disregarded the possibility of electron heating through superelastic collisions [process (1)].

In order to estimate the weight of each possible mechanism in heating electrons, we have calculated the heating rate of electrons through recombination and superelastic processes using the following relations:

$$P_{\mathrm{rec}}=n_e{}^2 n_{\mathrm{Ar}^+} \mathrm{k}_{\mathrm{rec}} \Delta E_{\mathrm{rec}} \tag{8}$$

and

$$P_{\mathrm{sup}}=n_e n_{\mathrm{Ar}^*} k_{\mathrm{sup}} \Delta E_{\mathrm{sup}}, \tag{9}$$

where ΔE_{rec} is taken equal to 0.15 E_i [11] (E_i=ionization energy=15.755 eV) and ΔE_{sup}=11.55 eV. The electron, ion,

TABLE IV. Calculated rate coefficients for e-H processes ($cm^3\ s^{-1}$). Letters a, b, c refer to the hypotheses as in the text and figures, numbers 1, 2, 3 to the three positions $x=2$, 4, 7 cm respectively. $n=2$ and $n=3$ are the excitation processes from $n=0$ to $n=1$ and $n=2$, while i is the ionization. Numbers in brackets represent powers of 10.

	$a1$	$b1$	$c1$	$a2$	$b2$	$c2$	$a3$	$b3$	$c3$
$K_{n=2}$	0.85[−26]	0.33[−11]	0.28[−11]	0.84[−26]	0.74[−12]	0.30[−12]	0.27[−26]	0.30[−12]	0.16[−14]
$K_{n=3}$	0.20[−31]	0.26[−13]	0.86[−13]	0.20[−31]	0.27[−14]	0.65[−14]	0.70[−32]	0.75[−15]	0.41[−16]
Ki	0.16[−38]	0.31[−13]	0.12[−12]	0.15[−38]	0.19[−14]	0.61[−14]	0.76[−39]	0.30[−15]	0.17[−16]

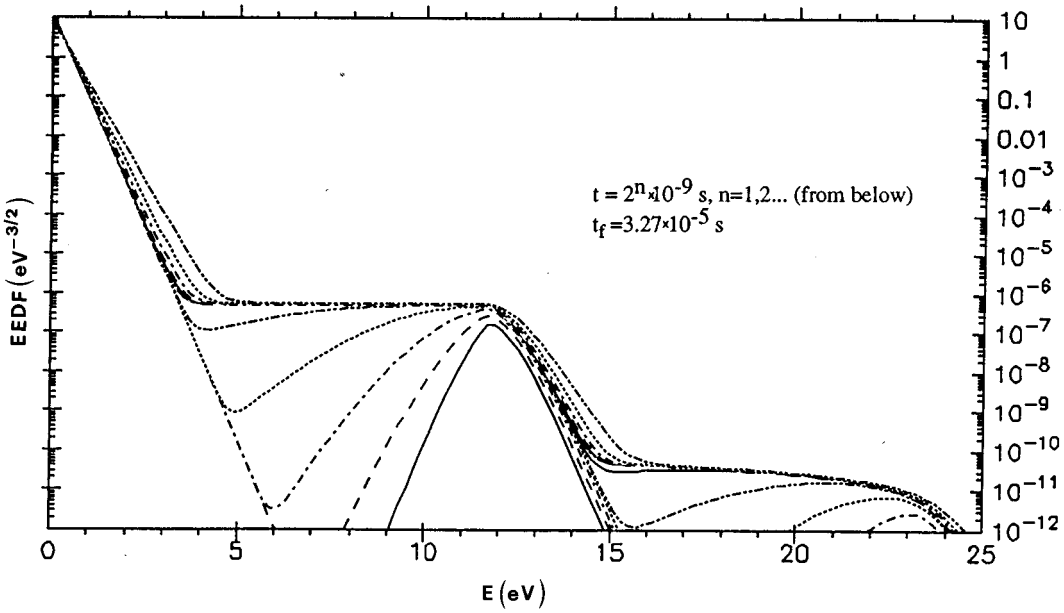

FIG. 5. EEDF calculated at different times for $x=20$ mm by solving the Boltzmann equation (2) for the hypothesis $c1$.

and metastable densities (n_e, n_{Ar^+}, n_{Ar*}) are those reported in Table I, while the electron temperatures at which we have calculated k_{rec} are the theoretical ones reported in the same table (see also Table I for the superelastic rates k_{sup}).

The results of this calculation have also been reported in Table I. We can see that the superelastic and recombination heating are of the same order of magnitude when we consider the low-temperature case (i.e., when we calculate P_{rec} at T_{e1}) while superelastic heating is orders of magnitude higher for the high-temperature case (i.e., when we calculate P_{rec} at T_{e2} and T_{e3}). In any case, the heating by superelastic collisions cannot be neglected.

Another possible source of the discrepancy between the experimental and calculated electron temperatures is the assumption of a steady state for EEDF. Indeed, the use of a stationary EEDF in describing the arc jet implicitly supposes that EEDF instantly reacts to the spatial evolution of the arc jet composition.

Calculation of the characteristic expansion times corresponding to Ref. [6] gives value orders of magnitude lower than the times necessary for the EEDF to achieve steady state (note that the total neutral density is of the order of 10^{15} cm^{-3}). A time-dependent solution of the Boltzmann equation may therefore be more appropriate for understanding the problem. The corresponding results (relative to the first position) have been reported in Fig. 5.

As an initial condition, we have assumed a Maxwell distribution at $T_e=0.2$ eV and a gas temperature of 3000 K. Then we follow the time evolution of EEDF. The reported EEDF's correspond to the times given by the formula $t=2^n\times10^{-9}$ s; the latest reported EEDF is for $t=3.27\times10^{-5}$ s and gives an electron average energy of 0.49 eV. The energy balance shows that at this time the EEDF is still far from the steady state. An estimate of the relaxation time of electron-neutral energy transfer for the investigated conditions gives approximately $\tau_{en}=10^{-3}$ s. Electron-ion collisions can speed up the energy exchange, but only at very low electron energies.

We see that for the expansion characteristic times of the investigated arc jet ($\tau_{exp}=10^{-5}$ s) a long plateau is formed by superelastic electronic collisions for intermediate electron energies (5 eV$<\varepsilon<$12 eV), while the bulk of low-energy electrons ($\varepsilon<5$ eV) satisfies a Maxwell distribution function at a temperature slightly larger than the initial one. The EEDF is, however, continuously evolving. In fact, *e-e* collisions tend to eliminate the plateau, which completely disappears at times of the order of 10^{-3} s. This last value represents an estimate of the time necessary for reaching the steady state EEDF of Fig. 1. This time-dependent calculation also shows that despite the strong cooling of *e-i* collisions, the electron temperature is continuously increasing during the evolution of the EEDF. The results of Fig. 5 can be, in any case, considered a clear indication of the importance of a time-dependent solution of the Boltzmann equation for understanding EEDF's under expanding arc conditions. The corresponding rates evolve following the time evolution of EEDF. As an example, the excitation rate of the Ar metastable state increases from approximately zero at $t=0$ to a value of 1.25×10^{-15} cm^3/s for $t=3.27\times10^{-5}$ s. Unfortunately the experiments do not report rates for both stationary and time-dependent conditions.

IV. CONCLUSIONS

In this paper we have shown, by solving both a stationary and a time-dependent Boltzmann equation, the importance of superelastic electronic collisions in affecting EEDF's and related properties in expanding arc conditions. Under stationary conditions the effect of superelastic collisions on the EEDF is masked by the spreading action of *e-e* collisions. In particular, the structures and plateaus that characterize the effects of the superelastic collisions can be completely removed by the action of *e-e* collisions. The time-dependent calculations show at early times the effect of superelastic collisions on the investigated arc jet EEDF, which exhibits a long plateau for energy between 5 and 12 eV.

However, for both stationary and time-dependent solutions, the EEDF retains the memory of the presence of superelastic collisions by an increase of the average energy (compared to the case in which these collisions are neglected) with dramatic consequences concerning the relevant rate coefficients.

Problems, however, arise when comparing theoretical and experimental electron temperatures. A satisfactory agreement is only found when we compare the slope of the EEDF in the very low-energy part of the distribution (i.e., T_{e1}), while a substantial discrepancy is found when we compare T_{e2} and T_{e3} with the experimental results.

Of course this point needs further experimental and theoretical investigation. From the theoretical point of view, one should solve at least a one-dimensional problem, which takes into account the coupling between the species transport and the electron Boltzmann equation. In this case, the species transport equations have to take into account the coupling between convection, diffusion, and chemical processes.

It should be noted that the shape of the calculated EEDF may strongly change the kinetics of excited states under expanding arc conditions. In fact, the assumption of a Maxwell distribution at the experimental T_e, completely rules out the importance of excitation processes from the ground state in populating excited states for both Ar and H atoms. As a consequence, the arc jet species kinetics seems to be completely controlled by three-body recombination processes, as suggested by Otorbaev *et al.*

Actually, if we consider the EEDF and the rate coefficients calculated in steady state (i.e., those of Figs. 1–3 and Tables II–IV), we can no longer neglect the excitation processes from the ground state compared to recombination processes. On the other hand, if use is made of the EEDF of Fig. 5 for calculating the relevant rate coefficients, we can expect that, despite the fact that the theoretical rate coefficients are much higher than those calculated with a Maxwell distribution function at the experimental electron temperature, the recombination processes may prevail in the excitation processes from the ground state.

In conclusion, the modeling of the expanding arc systems poses new conceptual problems because of the variety of dynamic and kinetic effects to be considered, but especially due to the discrepancy between experimental results and calculations based on the present physical background and modeling techniques. This system could represent an application for fluid dynamic methods, to account for the gas cooling during the expansion, and particle-in-cell methods to account for the space-charge field and plasma dynamics.

ACKNOWLEDGMENTS

This work has been partially supported by ASI (Agenzia Spaziale Italiana). One of the authors (M.C.) thanks the Université de Paris–Nord for supporting his stay in Paris, during which this work was started.

[1] S. D. Rockwood, Phys. Rev. A **8**, 2348 (1973).
[2] R. Winkler, J. Wilhelm, M. Capitelli, and C. Gorse, Plasma Chem. Plasma Process. **12**, 71 (1992).
[3] M. Capitelli, C. Gorse, J. Wilhelm, and R. Winkler, Lett. Nuovo Cimento **32**, 225 (1981).
[4] G. Capriati, G. Colonna, C. Gorse, and M. Capitelli, Plasma Chem. Plasma Process. **12**, 237 (1992).
[5] G. Colonna, C. Gorse, M. Capitelli, R. Winkler, and J. Wilhelm, Chem. Phys. Lett. **5**, 213 (1993).
[6] D. K. Otorbaev, A. J. Buuron, N. T. Guerissimov, M. C. M. Van de Sanden, and D. C. Schram, J. Appl. Phys. **76**, 4499 (1994); R. F. G. Meulembroeks, M. F. M. Steenbakkers, Z. Qing, M. C. M. Van de Sanden, and D. C. Schram, Phys. Rev. E **49**, 2272 (1994).
[7] M. Capitelli, G. Colonna, K. Hassouni, and A. Gicquel, Chem. Phys. Lett. **228**, 687 (1994); Plasma Chem. Plasma Process. **16**, 193 (1996).
[8] S. J. Buckmann and A. V. Phelps, JILA Information Center Report No. 27, University of Colorado, Boulder (1985).
[9] M. Capitelli and M. Dilonardo, Z. Naturforsch. **34**a, 585 (1979).
[10] W. L. Morgan and B. M. Penetrante, Comput. Phys. Commun. **58**, 127 (1990).
[11] R. F. G. Meulembroeks, R. A. H. Engeln, M. N. A. Beurskens, R. M. J. Paffen, M. C. M. Van Sanden, J. A. M. van der Mullen, and D. C. Schram, Phys. Rev. E **49**, 4397 (1995).